energies

MDPI

Article

A Redundancy Mechanism Design for Hall-Based Electronic Current Transformers

Kun-Long Chen [1,*], Ren-Shuo Wan [2], Yi Guo [3], Nanming Chen [2] and Wei-Jen Lee [4]

1 College of Electrical Engineering and Automation, Fuzhou University, Fuzhou 350116, China
2 Department of Electrical Engineering, National Taiwan University of Science and Technology, Taipei 106, Taiwan; m10307123@mail.ntust.edu.tw (R.-S.W.); nmchen@mail.ntust.edu.tw (N.C.)
3 Department of Mechanical Engineering, University of Texas at Dallas, Richardson, TX 75080, USA; Yi.Guo2@utdallas.edu
4 Department of Electrical Engineering, University of Texas at Arlington, Arlington, TX 76019, USA; wlee@uta.edu
* Correspondence: d9507103@mail.ntust.edu.tw; Tel.: +1-469-332-1192

Academic Editor: K.T. Chau
Received: 21 January 2017; Accepted: 28 February 2017; Published: 6 March 2017

Abstract: Traditional current transformers (CTs) suffer from DC and AC saturation and remanent magnetization in many industrial applications. Moreover, the drawbacks of traditional CTs, such as closed iron cores, bulky volume, and heavy weight, further limit the development of an intelligent power protection system. In order to compensate for these drawbacks, we proposed a novel current measurement method by using Hall sensors, which is called the Hall-effect current transformer (HCT). The existing commercial Hall sensors are electronic components, so the reliability of the HCT is normally worse than that of the traditional CT. Therefore, our study proposes a redundancy mechanism for the HCT to strengthen its reliability. With multiple sensor modules, the method has the ability to improve the accuracy of the HCT as well. Additionally, the proposed redundancy mechanism monitoring system provides a condition-based maintenance for the HCT. We verify our method with both simulations and an experimental test. The results demonstrate that the proposed HCT with a redundancy mechanism can almost achieve Class 0.2 for measuring CTs according to IEC Standard 60044-8.

Keywords: coreless Hall-effect current transformer (HCT); current measurement; current transformer (CT); Hall sensor; multiple sensor module; redundancy

1. Introduction

The smart grid is regarded as the next generation of power system, and substation intelligentization is a key technology in smart grids [1,2]. Regarding the commonly accepted current measurement methods in substation automation, traditional current transformers (CTs) are placed in a gas-insulated switchgear (GIS) to measure the currents, and their outputs are delivered through copper wires to intelligent electronic devices (IEDs) [3]. Practically speaking, traditional CTs encounter several technically unsolved problems (e.g., DC and AC saturation, remanent magnetization). These problems are all caused by the effect of hysteresis of CT iron cores [4,5]. Traditional CTs also have some physical drawbacks such as large volume and heavy weight, which limits the development and application of power protective systems. In order to solve the saturation problem and speed up substation intelligentization, electronic current transformers (ECTs), a method utilizing new semiconductor materials to design novel sensing technologies, have become one of the main research directions in measurement technologies [6–9]. Nowadays, some ECT technologies are commercialized, and related standards such as International Electrotechnical Commission (IEC) 61850 have been issued for

standardize the data processing, data acquisition, data transmission, and application framework in intelligent substations [10,11]. Table 1 presents a comparison between traditional CTs and ECTs. ECTs are classified into two types: active ECTs and passive ECTs. In the active ECTs, an external source is required to drive the sensing component. The typical techniques for active ECTs are Rogowski coil CT [12], low power CT (LPCT) [13], and magnetic-field-sensor-based CT [14]. For passive ECTs, the sensing components are unnecessary to have a driving source, and the representative technique is Faraday effect CT or optical CT (OCT) [15]. OCTs can maintain a good linearity in a wide current range, but their sensing structure is complicated and costly. Rogowski coil CTs cannot measure DC currents and are affordable but still not cheap enough. The sensing principle of LPCTs is the same as the traditional CTs, but the iron cores of LPCTs are manufactured using microcrystal alloy. Thus, LPCTs can achieve measurement accuracy with a smaller product volume due to the high permeability of microcrystal alloy. However, LPCTs are still heavy, and cannot measure DC currents. Regarding magnetic-field-sensor-based CTs, the commonly accepted sensing principles are anisotropic magneto resistance (AMR), giant magneto resistance (GMR), and the Hall effect [16]. Based on the Lorentz force, Hall sensors have a fast response time, a wide magnetic field measurement range, and good linearity. Both GMR and AMR originate from the magneto resistance effect, and their resistance values are sensitive to the varying measured magnetic fields. In the actual design, the configuration, which employs a Wheatstone bridge with AMR or GMR sensors, is mainly used in current measurement [17]. AMR and GMR sensors have a quick response time and are able to measure a wide current range. However, the linearity of AMR sensors is better than that of GMR sensors. The above three magnetic field sensors are all suitable for the current measurement. Nowadays, the integrated circuit (IC) technology-based Hall sensors are well developed. In this case, several compensation circuits can be integrated into Hall sensors to enhance the sensitivity and guarantee the steady performance [18]. Also, plenty of practical applications of the Hall sensors demonstrate their economic efficiency and that of related products.

Table 1. Summary of the main current sensing technologies.

	Traditional CT	Rogowski Coil CT	OCT	LPCT	Traditional Hall-Effect CT	Proposed Hall-Effect CT
Saturation problem	Yes	No	No	No	Yes	No
DC capable	No	No	Yes	No	No	No
Multifunction [1]	No	Yes	Yes	Yes	No	Yes
Range	A–kA	A–MA	A–MA	A–kA	mA–kA	A–MA
Linearity	Medium	Medium	Good	Good	Good	Good
Sensing structure	Simple	Simple	Complicated	Simple	Simple	Simple
Cost	Medium	Medium	Expensive	Medium	Medium	Low

[1] Multifunction: Multifunctional current measurements for metering and protective purposes.

Most sensing components within ECTs are semiconductor materials, meaning the reliability of ECTs would be worse than that of traditional CTs. Our study focuses on proposing a new redundancy mechanism for the coreless Hall-effect current transformer (HCT) [19] to enhance its reliability. The HCT is a sort of ECT, which places four Hall sensors symmetrically around the measured cable. Based on this sensor placement, the HCT can eliminate the ambient magnetic-field interference. Since there are no iron cores involved, the HCT would not encounter saturation when measuring a large current. In fact, the Hall sensor is also an electronic component, so it is not as reliable as the traditional CT. If one of the four Hall sensors fails, the HCT would not function well, which marks a weakness of HCTs as insufficient persistence. To enable the HCT have sufficient reliability for practical usage, we propose a new redundancy mechanism method. Multiple sensor modules are utilized in this method, and each sensor module consists of multiple Hall sensors. Besides, the algorithm designed for the proposed redundancy mechanism comprises three function units: (1) sensor module condition detection; (2) current measurement; and (3) sensor module failure alarm. First, the

sensor module condition detection function unit performs real-time sensor module condition detection. Then, the proper sensor modules are recognized. Finally, the outputs of all proper sensor modules are allowed to be sent to the current measurement function unit to calculate the measured current. The current measurement function unit can average the outputs of all proper sensor modules, and then the average Hall voltage is transformed into an actual current waveform. The current measurement function unit could also further improve the accuracy of the measurement, since the multiple sensor modules can compensate for the measurement error. Moreover, the sensor module failure alarm function unit receives a real-time report from all sensor module conditions. If one sensor module fails, the first phase of alarm will be visualized in the monitoring system, and the failed sensor module is also indicated. If two sensor modules fail, the second phase of alarm will be visualized in the monitoring system; meanwhile, the maintenance engineer is immediately informed to arrange a HCT replacement.

In a word, the redundancy mechanism monitoring system could achieve condition-based maintenance for the HCT, and this maintenance strategy can improve the entire measurement system's reliability and decrease the maintenance costs.

Note that the proposed HCT is mainly placed in the GIS, so the installation environment is steady without dramatic temperature change. Hence, the study is meant to develop a new redundancy mechanism for the HCT, and its measurement performance is our main concern. Additionally, in contrast to other similar industrial applications, the proposed HCT with a redundancy mechanism combines a temperature compensation mechanism, which will enable the system to perform well in a harsh environment. The system could remain stable even if the installation environment has dramatic temperature change.

The remainder of this paper is organized as follows. Section 2 assesses the amount of sensor modules and analyzes the sensing structure. In Section 3, a series of simulations are carried out to estimate the measurement accuracy of the HCT with a redundancy mechanism in a three-phase system. Section 4 describes the design and the implementation of proposed redundancy mechanism. In Section 5, lab experiments using a three-phase current measurement system are presented. Finally, this paper is concluded in Section 6.

2. Hall-Based Electronic Current Transformer

When an energized semiconductor is placed in a magnetic field space, moving charge carriers will gather in both sides of the original moving path due to the Lorentz force. Hence, there will be an electric field existing between both sides of the semiconductor. Finally, a potential difference, called Hall voltage, will be formed due to the electric field [20]. Hall sensors are often applied for physical detection, such as for magnetic field, current, position, angle, rotation speed, and direction. Generally, sensing materials of the commercial Hall sensors are mainly InSb, InAS, GaAs, Ge, and Si, and InSb, and GaAs demonstrates the best performance. Also, regarding the Si-based Hall sensor, the integrated circuit with built-in compensation circuits can reduce output noise and strengthen sensitivity [21]. Hence, Si becomes a widely used material for Hall sensors. In recent years, published research works related to Hall sensors can be classified into two parts: sensor property enhancement and application performance improvement. Since the sensitivity and the quiescent output voltage of Hall sensors are influenced by the ambient temperature, a few previous works [22,23] focused on how to resolve the thermal drift problems. Additionally, current measurement is one of the main applications related to Hall sensors, and most researches focused on the small current measurement [24] or the large current (fault current) measurement in the three-phase power systems [19,25].

When an electric current flows through a power cable, there is a magnetic field around the power cable and the magnetic field intensity is directly proportional to the current waveform magnitude. Some technologies based on Hall sensors have been proposed for current measurement, called Hall-effect transducers [24,26]. However, these transducers still strongly depend on iron cores, so the problem of core saturation cannot be avoided. The size of these transducers is almost the same as the bulk volume of traditional CTs. Furthermore, the authors in [27] proposed a Hall-effect current measurement method

without iron cores. However, this method integrated a measured conductor and Hall sensor into a common printed circuit board. Thereby, its isolation and anti-interference ability are not sufficient.

In a three-phase power system, there is serious magnetic field interference in the space. Regarding the designs concentrating on the magnetic field measurement without using iron cores, the previous works [19,28] recently proposed a coreless Hall-effect current transformer, called an HCT. In this design, four Hall sensors are placed symmetrically around the measured cable without an iron core, and the ambient magnetic field interference can be effectively eliminated by averaging the outputs of these four Hall sensors. Finally, the measured current can be accurately calculated by using the Biot-Savart Law for a long, straight cable. The formula is shown in (1) [29]

$$B = \frac{\mu_0 I}{2\pi r}(T) \tag{1}$$

where r is the distance between the center of the measured cable and the Hall sensor, B denotes the magnetic flux density at the distance r from the measured cable center, I is the measured current, and μ_0 denotes the permeability of free space.

In fact, some studies [30–32] also proposed symmetrical arrangement methods to improve the accuracy of current measurement with different kinds of magnetic field sensors. However, a three-phase system is not taken into consideration. The magnetic-field interference in the substation, especially from other two phase currents, has not been analyzed when designing the current sensors. Additionally, one study [33] presented a current measurement for three-phase busbars using magnetic sensor arrays, but the method requires a complicated optimization of the sensor positions and orientations using the D-optimality criterion and particle swarm optimization (PSO) technique.

Based on the sensing technology of the HCT, we developed a novel HCT with a redundancy mechanism. The proposed HCT consists of multiple sensor modules, and each sensor module consists of four Hall sensors, a weighted adder, and a voltage follower as shown in Figure 1. Four Hall sensors are utilized to measure the magnetic field produced by the measured current, and then the weight adder performs the average operation of the outputs from the four sensors. Finally, in order to avoid the load effect, a voltage follower is placed between the output of the weighted adder and the back-end data acquisition system. Moreover, the proposed HCT is meant for a 110 kV power system with a rated current of 600 A.

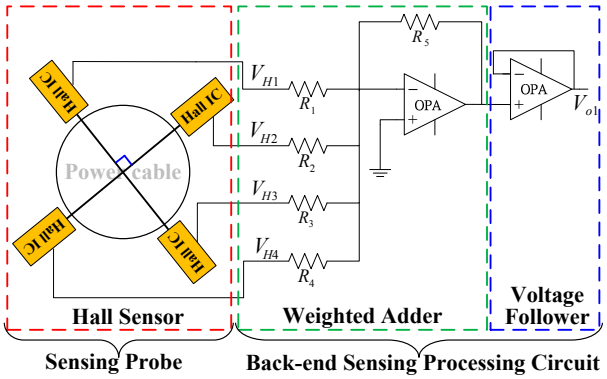

Figure 1. Sensor module for the proposed HCT.

3. Design of Redundancy Mechanism for the Proposed HCT

To enhance the reliability of the measurement system, the study uses multiple sensor modules to design the redundancy mechanism for the proposed HCT. In each sensor module, if a single Hall sensor cannot function well, the output of this sensor module will be removed from the measured current calculation. The HCT would perform the average of all waveforms generated by the rest of the sensor modules which work properly. The design of redundancy mechanism can also compensate

for the HCT measurement errors, meaning the accuracy of the proposed HCT will be guaranteed and improved.

Before designing the redundancy mechanism, this study analyzes the potential options for the HCT sensing structure (e.g., single layer and double layers) and assesses the accuracy and reliability of sensor modules. In order to increase the simulation's realism, the real noise of Hall sensors is added. Twenty-four Hall sensors are tested to measure the noises. The results are as shown in Figure 2. There are three noises distributed above the blue dotted line, and sensor index for these three results are 2, 3, and 21. Since these three noises are significantly larger than others, which could be regarded as outliers, they will not be involved in the simulation. After removing the noise outliers, we gather the twelve largest noises from the twenty-one sensors in Figure 2 to conduct the simulation.

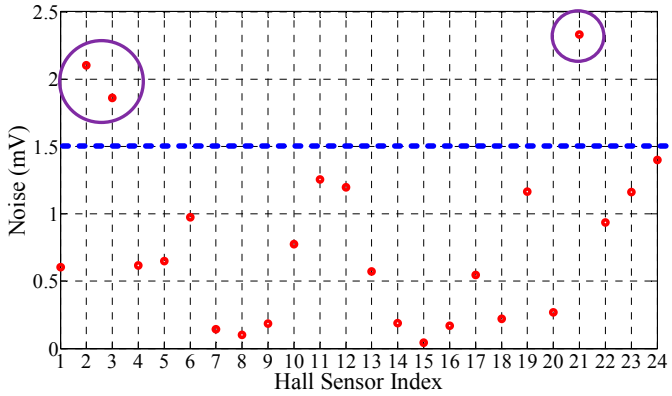

Figure 2. Noise measurement from each Hall sensor.

3.1. Sensing Structure and Sensor Module Amount

Concerning the sensing structure for multiple sensor modules, the study proposes two designs: single-layer structure and double-layer structure. The two designs are analyzed in a single-phase system. Moreover, the power cable geometry used in the simulation refers to an actual 100-kV GIS specification. The distance between two phases is 0.274 m, the cable radius is 0.015 m, and the rated current is 600 A.

3.1.1. Double-Layer Sensing Structure

The proposed double-layer sensing structure is shown in Figure 3. The measured cable is located in the center of the ECT. There are two concentric-circle sensing layers, and each layer has three sensor modules. In these two layers, each sensor module consists of four Hall sensors, which are marked in the identical colors and distributed symmetrically around the measured cable. There is a gap between the measured cable and the internal layer due to the insulation requirement.

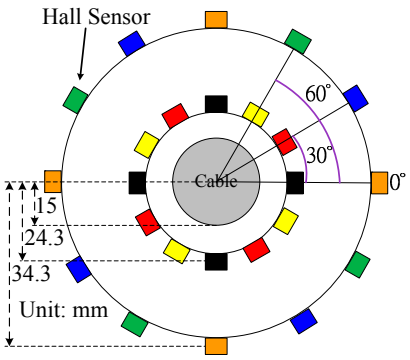

Figure 3. Design of double-layer sensing structure.

In this subsection, all sensing structure failure situations are taken into consideration when estimating the accuracy of the HCT. However, there are too many scenarios of double-layer sensing structure failure. Therefore, actual sensor errors are ignored in the simulation. The simulation results are shown in Table 2. The accuracy of the external-layer sensor modules is inferior to the accuracy of the internal-layer sensor modules. In particular, Case 15 only preserves one proper sensor module in the external layer, which provides the largest error in Table 2. Consequently, if there are proper sensor modules working in both layers simultaneously, the external-layer sensor module may result in the degradation in the accuracy of the HCT.

Table 2. Current errors of the proposed HCT with double-layer sensing structure in different sensor module failure situations.

Case	Sensor Module Failure		Current Error (%)
	Internal	External	
1	0	0	0.0000
2	0	1	0.0031
3	1	0	0.0008
4	0	2	0.0123
5	1	1	0.0038
6	2	0	0.0031
7	0	3	0.0000
8	1	2	0.0131
9	2	1	0.0062
10	3	0	0.0000
11	1	3	0.0015
12	2	2	0.0154
13	3	1	0.0061
14	2	3	0.0062
15	3	2	0.0245

3.1.2. Single-Layer Sensing Structure

The external-layer sensing module is not able to improve the accuracy of the HCT, and the double-layer structure requires a sophisticated back-end circuit and costs more. Therefore, to address the above concerns, we redesigned the sensing structure. In this new design, called a single-layer sensing structure, the external layer is removed. Only the internal layer with three sensor modules is retained. Moreover, actual sensor errors are added to simulate reality. The accuracy of the proposed HCT with a single-layer sensing structure is assessed according to IEC 60044-8 [34]. According to the accuracy class test requirement listed in IEC 60044.8, the test items include 5%, 20%, 100%, and 120% of the rated current (30 A, 120 A, 600 A, and 720 A, respectively). In fact, the test of 5% rated current is the most difficult due to the signal-to-noise ratio (SNR). Therefore, only the accuracy of the proposed HCT in the 5% rated current is shown in Table 3. The proposed HCT with a single-layer sensing structure can satisfy Class 0.2 in each case. When two or more proper sensor modules exist, the current error can be corrected, and then the accuracy of the HCT can be improved. Even though only one sensor module works properly, the accuracy of the HCT can still keep the same class. Hence, the reliability of the HCT is promoted and its persistence is lengthened as well.

Table 3. Current errors of the proposed HCT with single-layer sensing structure in different sensor module failure situations when tested current is 5% of rated current.

Case	Sensor Module Failure	Current Error (%)	IEC 60044-8 Class 0.2 (%)
1	0	0.0810	0.75
2	1	0.1699	
3	2	0.4943	

3.2. Single-Layer Sensing Structure in a Three-Phase System

3.2.1. Balanced Three-Phase System

Without iron cores, the most serious magnetic-field interference in an HCT originates from another two phase currents. After redesigning the HCT sensing structure, the HCT accuracy could be evaluated in an actual three-phase system. As shown in Figure 4, three-phase cables are arranged in a triangular form, and each phase cable is considered as a long straight conductor. Three-phase currents are defined as $i_R = I_m \cos(\omega t)$, $i_S = I_m \cos(\omega t - 120^\circ)$, and $i_T = I_m \cos(\omega t + 120^\circ)$. The distance d between any two phases is settled according to an actual 110-kV GIS with the rated current of 600 A. We only demonstrate the results for 5% rated current in Table 4, since this scenario is hard to carry out regarding the SNR issue. From the results in Table 4, we conclude that the proposed HCT with a single-layer sensing structure can satisfy Class 0.2 in each case. With the design of multiple sensor modules, the accuracy of the proposed HCT can always keep the same class even though only one sensor module works properly. Hence, the reliability of the HCT is guaranteed and its persistence is improved as well.

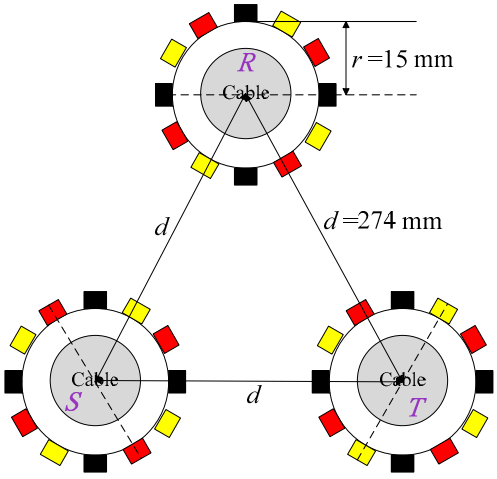

Figure 4. Geometry of three-phase cables and arrangement of sensor modules.

Table 4. Current errors of the proposed HCT when three-phase currents are balanced and are 5% of rated current.

Case	Sensor Module Failure	Current Error (%)			IEC 60044-8 Class 0.2 (%)
		R Phase	*S* Phase	*T* Phase	
1	0	0.0809	0.0807	0.0809	0.75
2	1	0.1676	0.1672	0.1675	
3	2	0.4850	0.4844	0.4849	

3.2.2. Unbalanced Three-Phase System

When a single line-to-ground fault occurs, the fault current will cause the most serious magnetic field interferences among phases. In this simulation, we assume a single line-to-ground fault occurs in the *R* phase, and the fault current is up to 18 kA. In steady state, the *R* phase current is full-load current and other two phase currents are quarter-load current. The simulation results are listed in Table 5. The maximum composite error of the proposed HCT is smaller than 5% in each case when the fault current is 30 times than the rated current. From the simulation results, we could conclude that with the design of multiple sensor modules, the accuracy of the proposed HCT can still maintain the Class 5P30 for the protective CT, even if only one sensor module works properly.

Table 5. Maximum composite errors of the proposed HCT when three-phase currents are unbalanced and a single-to-line fault occurs in *R* phase.

Case	Sensor Module Failure	Maximum Composite Error among Three Phases (%)	IEC 60044-8 Class 5P30 (%)
1	0	−0.02	
2	1	−0.17	5
3	2	0.2	

4. Implementation of the Redundancy Mechanism

4.1. Hardwire

The implementation of the proposed redundancy mechanism is shown in Figure 5. The hardwire design contains three sensor modules, a voltage regulator and a redundancy mechanism monitoring system. Each sensor module consists of four Hall sensors and one back-end sensing processing circuit. As shown in Figure 1, the back-end sensing processing circuit contains a weighted adder and a voltage follower. The weighted adder averages the outputs from four Hall sensors. The average operation is defined in (2). A +5 V power source for Hall sensor and a ±12 V power source for the operational amplifier (OPA) circuit are all supplied by the voltage regulator. The voltage regulator is supplied by a DC power supply. The redundancy mechanism monitoring system is used to acquire all measured signals from sensor modules, and then perform the function algorithm of the redundancy mechanism based on LabVIEW software (2013 Full Development System, National Instruments, Austin, TX, USA).

$$\begin{aligned} V_{O1} &= -\left(\frac{R_5}{R_1}V_1 + \frac{R_5}{R_2}V_2 + \frac{R_5}{R_3}V_3 + \frac{R_5}{R_4}V_4\right) \\ &= -\tfrac{1}{4}(V_1 + V_2 + V_3 + V_4) \end{aligned} \quad (2)$$

where

V_1, V_2, V_3, V_4: Outputs of four Hall sensors.
R_1, R_2, R_3, R_4: 50 kΩ.
R_5: 10 kΩ.

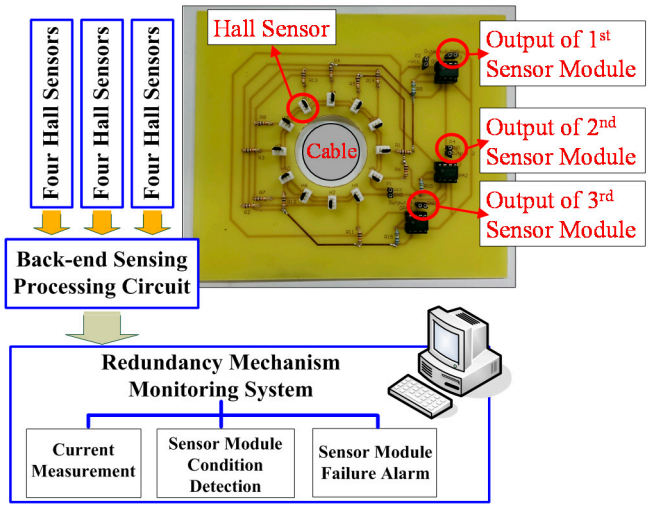

Figure 5. Implementation of the proposed HCT with redundancy mechanism.

4.2. Software

The LabVIEW-based redundancy mechanism monitoring system (2013 Full Development System, National Instruments, Austin, TX, USA) has three function units, including the sensor module condition detection, the measurement function, and the sensor module failure alarm. All units are introduced as follows:

4.2.1. Sensor Module Condition Detection Function Unit

The flowchart of the sensor module condition detection function unit is shown in Figure 6. The function unit determines the sensor module conditions by detecting the DC level of Hall voltages. During the normal operation, the DC level of the selected Hall sensors is limited between 2.4 V and 2.6 V [35]. We settle this range as a reference to determine the sensor module conditions. When the DC level of Hall voltage output from the sensor module is detected to be out of the reference, this Hall voltage is isolated and is not used for the final average calculation. In the meantime, the detection results are reported to the monitoring system. The failed sensor module will be marked in the human machine interface (HMI) panel.

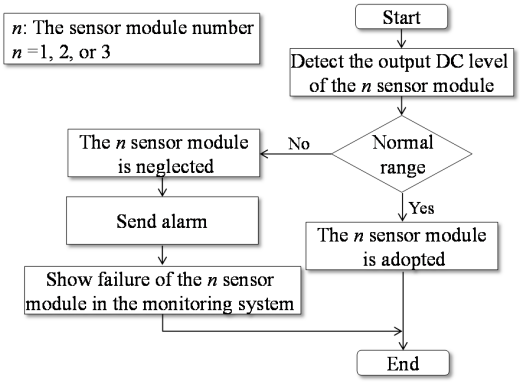

Figure 6. Flowchart of sensor module condition function unit.

4.2.2. Current Measurement Function Unit

The flowchart of the current measurement function unit is shown in Figure 7. First, the function unit reads Hall voltages output by sensor modules which are measured by the data-acquisition card. The magnetic fields are calculated from the Hall voltages according to the Hall-sensor sensitivity. Then, the current measured by each sensor module is calculated based on the magnetic fields using (1). Based on the result of the sensor module condition detection function unit, only the calculated currents from the proper sensor modules are adopted for the final average calculation. The final average value is defined as the measurement result of the proposed HCT.

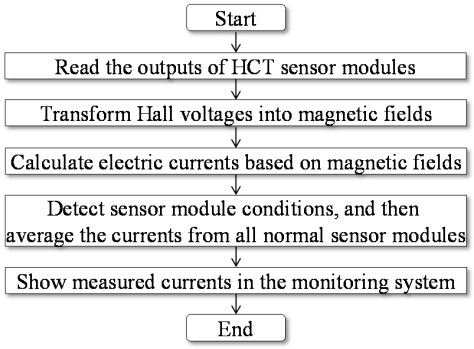

Figure 7. Flowchart of current measurement function unit.

4.2.3. Sensor Module Failure Alarm Function Unit

The flowchart of the sensor module failure alarm function unit is shown in Figure 8. This function unit should go with the sensor module condition function unit to implement the failure alarm. The monitoring system checks each sensor module condition during the normal operation. When detecting any single failed sensor module, the monitoring system shows the first phase of alarm and indicates the failed sensor module. In the case of finding two failed sensor modules, the monitoring system shows the second phase of alarm and the maintenance engineer is immediately notified to arrange an HCT replacement.

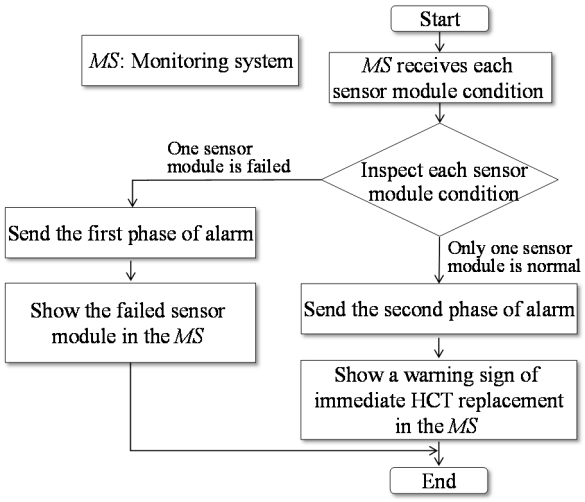

Figure 8. Flowchart of sensor module failure alarm function unit.

5. Measurement Results and Discussion

A three-phase current measurement system is designed to test the proposed HCT with the redundancy mechanism. As shown in Figure 9, three single-phase autotransformers are used to energize other three transformers. The secondary winding of the second transformer is only one turn. When this turn is closed, the secondary winding can produce a large current. The distance between any two phases is settled to be 0.274 m according to a 110-kV GIS. The rated current is 600 A. The proposed HCT is installed in *R* phase to test its accuracy class in the single-phase system and in the three-phase system. During the tests, a Class-0.1 and 600/5-A traditional CT is selected as a reference instrument.

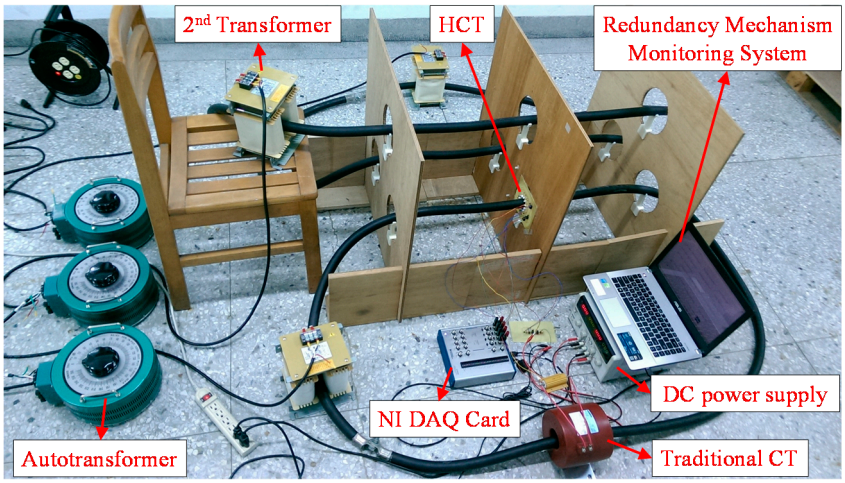

Figure 9. Measurement system framework.

5.1. Single-Phase Current Measurement

In the test of the single-phase current measurement, only the *R* phase is energized to produce the testing current. The measurement results, including outputs from all sensor modules and the HCT in all sensor module failure conditions, are listed in Table 6. In order to simplify the discussion in all experiments, one sensor module failure means that the 3rd sensor module fails; two sensor modules failure means the 2nd and 3rd sensor modules fail. From the results in Table 6, the accuracy of each sensor module satisfies the Class 0.5 requirements, and the accuracy of the proposed HCT without any failed sensor module can almost achieve Class 0.2. If one or two sensor modules fail, the proposed HCT can still guarantee Class 0.5. Therefore, we could conclude that our design for the redundancy mechanism not only extends the life time of the proposed HCT, but also improves the accuracy class of the proposed HCT in case of module failure.

Table 6. Current errors of the proposed HCT when only the *R* phase is energized to produce testing current.

Accuracy Class	**Percentage Current Error (%) at Percentage of Rated Current Shown Below**			
	5%	**20%**	**100%**	**120%**
Class 0.2 of IEC Standard 60044-8	±0.75	±0.35	±0.2	±0.2
Class 0.5 of IEC Standard 60044-8	±1.5	±0.75	±0.5	±0.5
Measurement result of each sensor module				
Sensor module 1	1.118	0.276	−0.00	−0.10
Sensor module 2	0.710	0.511	−0.00	−0.10
Sensor module 3	0.391	0.410	−0.01	−0.11
Sensor module failure	Proposed HCT with redundancy mechanism			
0	0.740	0.399	−0.00	−0.10
1	0.914	0.393	−0.00	−0.10
2	1.118	0.276	−0.00	−0.10

5.2. Balanced Three-Phase Current Measurement

Three-phase current measurement includes a balanced three-phase test and an unbalanced three-phase test. Regarding the balanced test, three-phase currents are settled to the rated current of 600 A. Test results are listed in Table 7. The current errors of the proposed HCT in the balanced three-phase current test are similar to the results of the single-phase current test. Hence, the proposed HCT with the redundancy mechanism is capable of resisting the three-phase magnetic field interference. Even in an extreme case, when only one sensor module can work properly, the accuracy of the HCT can still maintain the same class for the single-phase current measurement results.

Table 7. Current errors of the proposed HCT when three-phase currents are balanced.

Percentage Current Error (%) at 100% of Rated Current	
Measurement result of each sensor module	
Sensor module 1	−0.02
Sensor module 2	−0.01
Sensor module 3	−0.01
Sensor module failure	Proposed HCT with redundancy mechanism
0	−0.01
1	−0.02
2	−0.02

5.3. Unbalanced Three-Phase Current Measurement

Regarding the unbalanced three-phase current measurement, three phase currents tests are conducted in three scenarios, including (1) *R* phase: 600 A, *S* phase: 300 A, *T* phase: 150 A; (2) *R* phase: 300 A, *S* phase: 150 A, *T* phase: 600 A; (3) *R* phase: 150 A, *S* phase: 600 A, *T* phase: 300 A. The proposed HCT is installed in the *R* phase, and test results are listed in Table 8. The current errors in the unbalanced current tests are slightly larger than the results in the balanced tests. The reason is that other unbalanced two-phase currents suffer from serious magnetic field interference. Fortunately, the design of the redundancy mechanism has the ability to improve the HCT accuracy. In fact, even if only one sensor module can work properly, the error of HCT for the 600-A test in *R* phase can still be smaller than 0.2%.

Table 8. Current errors of the proposed HCT when three-phase currents are unbalanced.

Current	Scenario 1	Scenario 2	Scenario 3
R-Phase Current (A)	600	300	150
S-Phase Current (A)	300	150	600
T-Phase Current (A)	150	600	300
Percentage current error (%)			
Measurement result of each sensor module			
Sensor module 1	−0.03	−0.07	−0.38
Sensor module 2	−0.02	0.68	1.12
Sensor module 3	−0.03	0.26	0.32
Sensor module failure	Proposed HCT with redundancy mechanism		
0	−0.02	0.29	0.35
1	−0.03	0.30	0.36
2	−0.03	−0.07	−0.38

6. Conclusions

A novel redundancy mechanism for lengthening the life of the HCT is proposed in this paper. Multiple sensor modules are adopted to design a single-layer sensing structure. The function algorithm programmed into three units of the redundancy mechanism is implemented in the redundancy mechanism monitoring system. This monitoring system performs real-time sensor module condition detection. The monitoring system could achieve a condition-based maintenance for the proposed HCT, so the measurement system's reliability can be improved and guaranteed.

A series of tests have been conducted, which include a single-phase current and balanced/unbalanced three-phase currents. The test results demonstrate that the proposed redundancy mechanism can effectively improve the accuracy of the HCT and lengthen the lift time of the HCT as well, even if the system encounters extreme working conditions (e.g., only one sensor module working properly).

The main contributions of this research work are (1) a new redundancy mechanism for the HCT is proposed to increase its persistence and to promote its reliability; (2) condition-based maintenance is realized for the proposed HCT; (3) the proposed HCT with a redundancy mechanism can also improve the original measurement accuracy; (4) the proposed HCT with a redundancy mechanism can almost reach Class 0.2 according to the IEC standard 60044-8; (5) even if only one sensor module works properly, the HCT can still maintain Class 0.5; (6) the complete process of designing and implementing the redundancy mechanism are demonstrated; and (7) the proposed HCT with a redundancy mechanism has economic and volume advantages in terms of potentially replacing traditional CTs and other ECTs.

Acknowledgments: The work was supported by the Ministry of Science and Technology, Taiwan under Contract MOST 104-2221-E-011-071.

Author Contributions: Kun-Long Chen, Ren-Shuo Wan and Nanming Chen conceived and designed the method; all authors analyzed the data; Kun-Long Chen and Ren-Shuo Wan performed simulations and experiments; Kun-Long Chen and Wei-Jen Lee refined the algorithm Kun-Long Chen, Wei-Jen Lee and Yi Guo wrote the paper.

Conflicts of Interest: The authors declare no conflict of interest.

References

1. Yu, Y.; Yang, J.; Chen, B. The smart grids in China—A review. *Energies* **2012**, *5*, 1321–1338. [CrossRef]
2. Li, F.; Qiao, W.; Sun, H.; Wan, H.; Wang, J.; Xia, Y.; Xu, Z.; Zhang, P. Smart transmission grid: Vision and framework. *IEEE Trans. Smart Grid* **2010**, *1*, 168–177. [CrossRef]
3. McDonald, J.D. Substation automation. IED integration and availability of information. *IEEE Power Energy Mag.* **2003**, *1*, 22–31. [CrossRef]
4. Kasztenny, B.; Finney, D. Generator protection and CT-saturation problems and solutions. *IEEE Trans. Ind. Appl.* **2005**, *41*, 1452–1457. [CrossRef]
5. Ajaei, F.B.; Sanaye-Pasand, M.; Davarpanah, M.; Rezaei-Zare, A.; Iravani, R. Compensation of the current-transformer saturation effects for digital relays. *IEEE Trans. Power Deliv.* **2011**, *26*, 2531–2540. [CrossRef]
6. Cruden, A.; Richardson, Z.J.; McDonald, J.R.; Andonovic, I.; Laycock, W.; Bennett, A. Compact 132 kV combined optical voltage and current measurement system. *IEEE Trans. Instrum. Meas.* **1998**, *47*, 219–223. [CrossRef]
7. Kucuksari, S.; Karady, G.G. Experimental comparison of conventional and optical current transformers. *IEEE Trans. Power Deliv.* **2010**, *25*, 2455–2463. [CrossRef]
8. Ziegler, S.; Woodward, R.C.; Iu, H.H.; Borle, L.J. Current sensing techniques: A review. *IEEE Sens. J.* **2009**, *9*, 354–376. [CrossRef]
9. Ibrahim, M.E.; Abd-Elhady, A.M. Differential reconstruction method for power frequency AC current measurement using Rogowski coil. *IEEE Sens. J.* **2016**, *16*, 8420–8425. [CrossRef]
10. Yang, L.; Crossley, P.A.; Wen, A.; Chatfield, R.; Wright, J. Design and performance testing of a multivendor IEC61850-9-2 process bus based protection scheme. *IEEE Trans. Smart Grid* **2013**, *5*, 1159–1164. [CrossRef]
11. Yun, S.Y.; Chu, C.M.; Kwon, S.C.; Song, I.K.; Choi, J.H. The development and empirical evaluation of the Korean smart distribution management system. *Energies* **2014**, *7*, 1332–1362. [CrossRef]
12. Mohseni, H. The Rogowski coil principles and applications: A review. *IEEE Sens. J.* **2015**, *15*, 651–658.
13. Fluri, R.; Schmid, J.; Braun, P. Applications of low power current and voltage sensors. In Proceedings of the 21st International Conference on Electricity Distribution (CIRED), Frankfurt, Germany, 6–9 June 2011.
14. Popovic, R.S.; Drljaca, P.M.; Schott, C. Bridging the gap between AMR, GMR, and Hall magnetic sensors. In Proceedings of the 23rd International Conference on Microelectronics, Hammamet, Tunisia, 19–22 December 2011.
15. Samimi, M.H.; Akmal, A.A.S.; Mohseni, H. Optical current transducers and error sources in them: A review. *IEEE Sens. J.* **2015**, *15*, 4721–4728. [CrossRef]
16. Ripka, P. Electric current sensors: A review. *Meas. Sci. Technol.* **2010**, *21*, 1–23. [CrossRef]
17. Xie, F.; Weiss, R.; Weigel, R. Giant-magnetoresistance-based galvanically isolated voltage and current measurements. *IEEE Trans. Instrum. Meas.* **2015**, *64*, 2048–2054. [CrossRef]
18. Heidari, H.; Bonizzoni, E.; Gatti, U.; Maloberti, F. A CMOS current-mode magnetic hall sensor with integrated front-end. *IEEE Trans. Circuits Syst. I Regul. Pap.* **2015**, *62*, 1270–1278. [CrossRef]
19. Chen, K.L.; Chen, N. A new method for power current measurement using a coreless Hall effect current transformer. *IEEE Trans. Instrum. Meas.* **2011**, *60*, 158–169. [CrossRef]
20. Boero, G.; Demierre, M.; Besse, P.A.; Popovic, R.S. Micro-Hall devices: Performance, technologies and applications. *Sens. Actuators A* **2003**, *106*, 314–320. [CrossRef]
21. Huang, H.; Wang, D.; Xu, Y. A monolithic CMOS magnetic Hall sensor with high sensitivity and linearity characteristics. *Sensors* **2015**, *15*, 27359–27373. [CrossRef] [PubMed]
22. Huber, S.; Leten, W.; Ackermann, M.; Schott, C.; Paul, O. A fully integrated analog compensation for the piezo-Hall effect in a CMOS single-chip Hall sensor microsystem. *IEEE Sens. J.* **2015**, *15*, 2924–2933. [CrossRef]

23. Jiang, J.; Makinwa, K. A hybrid multi-path CMOS magnetic sensor with 76 ppm/°C sensitivity drift. In Proceedings of the 42nd European Solid-State Circuits Conference, Lausanne, Switzerland, 12–15 September 2016.
24. Ajbl, A.; Pastre, M.; Kayal, M. A fully integrated Hall sensor microsystem for contactless current measurement. *IEEE Sens. J.* **2013**, *13*, 2271–2278. [CrossRef]
25. Tsai, Y.P.; Chen, K.L.; Chen, N. Design of a Hall effect current microsensor for power networks. *IEEE Trans. Smart Grid* **2011**, *2*, 421–427. [CrossRef]
26. Cristaldi, L.; Ferrero, A.; Lazzaroni, M.; Ottoboni, R.T. A linearization method for commercial Hall-effect current transducers. *IEEE Trans. Instrum. Meas.* **2001**, *50*, 1149–1153. [CrossRef]
27. Frick, V.; Hebrard, L.; Poure, P.; Anstotz, F.; Braun, F. CMOS microsystem for AC current measurement with galvanic isolation. *IEEE Sens. J.* **2003**, *3*, 752–760. [CrossRef]
28. Chen, K.L.; Chen, Y.R.; Tsai, Y.P.; Chen, N. A novel wireless multifunctional electronic current transformer based on ZigBee-based communication. *IEEE Trans. Smart Grid* **2016**. [CrossRef]
29. Cheng, D.K. *Field and Wave Electromagnetics*; Addison-Wesley: Reading, MA, USA, 1989; pp. 226, 321–345.
30. Scoville, J.T.; Petersen, P.I. A low-cost multiple Hall probe current transducer. *Am. Inst. Phys.* **1991**, *62*, 755–760. [CrossRef]
31. Bazzocchi, R.; Rienzo, L.D. Interference rejection algorithm for current measurement using magnetic sensor arrays. *Sens. Actuators A* **2000**, *85*, 38–41. [CrossRef]
32. Mlejnek, P.; Vopálenský, M.; Ripka, P. AMR current measurement device. *Sens. Actuators A* **2008**, *141*, 649–653. [CrossRef]
33. Rienzo, L.D.; Zhang, Z. Spatial harmonic expansion for use with magnetic sensor arrays. *IEEE Magn.* **2010**, *46*, 53–58. [CrossRef]
34. International Electrotechnical Commission. *Instrument Transformers—Part 8: Electronic Current Transformers*; IEC Standard 60044-8; IEC: Geneva, Switzerland, 2002.
35. Allegro MicroSystems. *A1301 and A1302 Datasheets*; Allegro MicroSystems, Inc.: Worcester, MA, USA, 2016.